Stability and Mobility of Mono- and Di-Interstitials in α-Fe

Chu-Chun Fu and F. Willaime
Service de Recherches de Métallurgie Physique, CEA/Saclay, 91191 Gif-sur-Yvette Cedex, France

P. Ordejón
Institut de Ciència de Materials de Barcelona (CSIC), Campus de la U.A.B., 08193 Bellaterra, Spain
(Received 12 January 2004; published 30 April 2004)

We report a detailed *ab initio* study of the stability and migration of self-interstitial atoms (SIAs) and di-interstitials (di-SIAs) in α-Fe. The $\langle 110 \rangle$ dumbbell is confirmed to be the most stable SIA configuration, 0.7 eV below the $\langle 111 \rangle$ dumbbell. The lowest-energy migration path corresponds to a nearest-neighbor translation-rotation jump with a barrier of 0.34 eV. The most stable configuration for di-SIAs consists of $\langle 110 \rangle$ parallel dumbbells. Their migration mechanism is similar to that for SIAs, with an activation energy of 0.42 eV. These results are at variance with predictions from existing empirical potentials and allow one to reconcile theory with experiments.

DOI: 10.1103/PhysRevLett.92.175503 PACS numbers: 61.72.Ji, 31.15.Ar, 66.30.Lw, 67.80.Mg

Vacancies are the dominant self-defects at equilibrium in metals, but under irradiation self-interstitial atoms (SIAs) are produced in the same amount. Their energetic and kinetic properties determine the temporal defect-population evolution and consequent changes in material microstructure [1]. The properties of SIAs are by far less well known than those of vacancies, and many questions such as their diffusion characteristics are still open [2,3]. The behavior of SIAs is atypical in α-Fe with respect to other body centered cubic (bcc) metals since the migration energy is unusually large, i.e., 0.30 eV instead of at most 0.1 eV in other metals [4]. Studies based on empirical potentials predict that the $\langle 110 \rangle$ and $\langle 111 \rangle$ dumbbell configurations of SIAs are very close in energy, and that SIAs migrate via very fast one-dimensional $\langle 111 \rangle$ motion, combined with occasional thermally activated reorientations [5–7]. This widely accepted picture is questioned by recent *ab initio* calculations showing that the energy difference between the $\langle 110 \rangle$ and $\langle 111 \rangle$ dumbbells is much larger than expected, around 0.7 eV [8,9]. This large value makes a migration via the $\langle 111 \rangle$ dumbbell incompatible with the experimental value of SIA migration energy of 0.3 eV [4,10]. The identification of an alternative migration mechanism is the first goal of this work.

SIAs are highly mobile and attractive from each other, and they therefore tend to cluster. In contrast to other bcc metals, in α-Fe the Burgers vectors of the resulting dislocation loops are observed by transmission electron microscopy to be either $\frac{1}{2}\langle 111 \rangle$ or $\langle 100 \rangle$ instead of predominantly $\frac{1}{2}\langle 111 \rangle$ [11]. Some mechanisms have been proposed to explain this still unclear complex behavior [12,13]. Studies based on embedded-atom method (EAM) type empirical potentials predict that the most stable configurations for di-SIAs and larger SIA clusters are formed by parallel $\langle 111 \rangle$ dumbbells that exhibit very fast $\langle 111 \rangle$ motion [5–7,14]. This low migration-energy mechanism is incompatible with the 0.42 eV experimental value of the migration energy of small SIA clusters [10]. This discrepancy raises the question of the migration mechanism of small SIA clusters but also of their structure, starting with di-SIAs, and this is the second purpose of this Letter.

In view of the discrepancies between empirical potential results and experiments, the stability and mobility of SIAs and di-SIAs are investigated here by *ab initio* techniques, using the SIESTA method [15], which has been successfully applied to the study of many semiconducting and a few metallic systems [16,17]. The present calculations are spin-polarized and the Perdew-Burke-Ernzerhof generalized gradient approximation (GGA) scheme is used for exchange and correlation. Core electrons are replaced by nonlocal norm-conserving pseudopotentials with cutoff radii of 1.16 Å for s, p, and d orbitals and 0.37 Å for the partial core correction. Valence electrons are described by linear combinations of numerical pseudoatomic orbitals using a split-valence multiple-ζ basis set consisting of ten localized functions: two, one, and one shells for $4s$, $4p$, and $3d$ orbitals, respectively. These orbitals vanish outside a cutoff radius ≤ 2.95 Å. Including the $3s$ and $3p$ orbitals in the valence states has no significant effect on energy differences between SIA configurations, unlike, e.g., in Mo [18]. The charge density is represented on a regular real space grid of 0.08 Å. The Methfessel-Paxton scheme for electronic density of state broadening is used with a 0.3 eV width. Except when otherwise mentioned, all the results presented below are obtained using 128 ($+1$ or $+2$) atom cells and a $3 \times 3 \times 3$ shifted k-point grid with a full relaxation of the atomic positions and of the shape and size of the supercell. The residual forces and stress components are smaller than 0.04 eV/Å and 10 kbar, respectively. The error in system total energy due to real space grid, k point sampling, residual forces, and stresses is estimated to be about 0.1 eV. The migration-path

TABLE I. Comparison of bulk and vacancy properties in α-Fe: lattice parameter, a (in Å), bulk modulus, B (in Mbar), magnetic moment μ (in μ_B), vacancy formation and migration energies, E_f^v and E_m^v (in eV). The vacancy calculations are performed on $54(-1)$ atom supercells at constant volume. PW1 [8] and PW2 [20] denote DFT-GGA plane-wave results; the PW2 values correspond to two pseudopotentials.

	a	B	μ	E_f^v	E_m^v
This work	2.88	1.80	2.31	2.07	0.67
PW1 (VASP)	2.86	1.60	2.32	1.95	0.64
PW2 (PWSCF)	2.85	1.52–1.67	2.26–2.38	1.93–2.09	0.59–0.67
Experiment	2.87	1.68	2.22	2.0 ± 0.2	0.55

calculations are performed at a fixed volume [19] using the drag method; the atomic positions relative to the center of mass are constrained to relax in the hyperplane perpendicular to the vector connecting the initial and final positions.

The accuracy of the pseudopotential and basis set have been tested on some relevant bulk properties and on the monovacancy formation and migration energies. The agreement with experiments and plane-wave density functional theory (DFT)-GGA calculations is very satisfactory, the difference between present and plane-wave results [8,20] being similar to the effect of pseudopotentials (see Table I).

We have then calculated the formation energies of the following high symmetry SIA configurations: $\langle 110 \rangle$, $\langle 111 \rangle$, and $\langle 100 \rangle$ dumbbells, crowdion, tetrahedral, and octahedral (see, e.g., Ref. [18] for their representation). The comparison with $54 + 1$ atom supercell results shows that the calculation is well converged with respect to supercell size (Fig. 1): the differences in formation energies are negligible except for the $\langle 111 \rangle$ dumbbell and the crowdion, which are larger by only 0.1 eV in the largest supercell. This trend is fully consistent with calculations

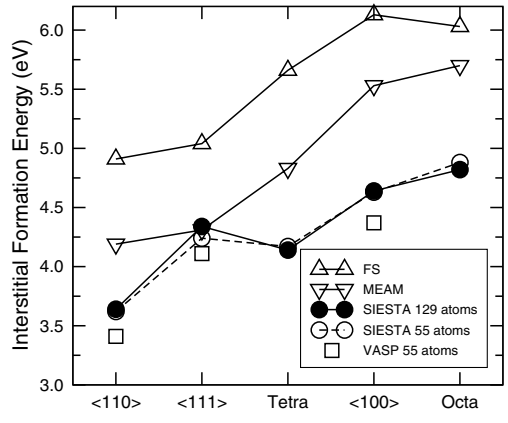

FIG. 1. SIA formation energies in α-Fe: comparison of the present SIESTA *ab initio* results for two supercell sizes with plane-wave (VASP) [8] and empirical potential (FS and MEAM) [21,22] calculations. The crowdion (not represented) is always nearly degenerate with the $\langle 111 \rangle$ dumbbell.

in bcc vanadium [18]. The comparison with plane-wave results on 55-atom cells for the dumbbell configurations [8] shows again a very good agreement between the two *ab initio* methods with a global shift in formation energy of about 5% (Fig. 1), confirming the validity of the present approach. The value of the Frenkel pair formation energy, deduced from the sum of vacancy and SIA formation energies (see Tables I and II), i.e., 5.69 eV, is in reasonable agreement with the experimental estimate of 6.3 to 6.6 eV [23]. This discrepancy may be partly due to the tendency of GGA to underestimate the vacancy formation energy [24], in particular, in α-Fe [20].

The lowest-energy configuration is found to be the $\langle 110 \rangle$ dumbbell, in agreement with experiments [2], followed by the tetrahedral, $\langle 111 \rangle$ and $\langle 100 \rangle$ dumbbells, and octahedral configurations which are, respectively, 0.50, 0.70, 1.00, and 1.18 eV higher in energy. The crowdion is practically degenerate with the $\langle 111 \rangle$ dumbbell. The rather large energy difference between the $\langle 111 \rangle$ and $\langle 110 \rangle$ dumbbell configurations reported in Ref. [8] is therefore fully confirmed.

These results contrast with those from two empirical potentials chosen here for their representative character: the first one, of Finnis-Sinclair (FS) type [21], has been widely used in molecular dynamics simulations of SIA loops and displacement cascades [5,7,14], and the second one, of the recent modified EAM (MEAM) type [22], accounts for angular forces that are important in bcc metals. Figure 1 clearly shows that, besides a global shift of the formation energies, the main discrepancy between empirical potentials and *ab initio* calculations is the large relative formation energies of $\langle 111 \rangle$ configurations predicted by the latter.

The dynamics of SIAs has then been investigated by studying various migration jumps up to third-nearest neighbors as well as on-site rotations (Figs. 2), starting from the $\langle 110 \rangle$ dumbbell. The activation energies are determined by the calculation of the full migration or rotation pathways. The most favorable migration mechanism is found to correspond to the nearest-neighbor translation-rotation jump [see Figs. 2(a) and 3], with a

TABLE II. Formation energies (in eV) of SIA and di-SIA dumbbell configurations, and comparison with experiments of the migration energies of $\langle 110 \rangle$ configurations. Di-SIA results include stability of first (1nn), second (2nn), and third (3nn) nearest-neighbor configurations, and migration energies for the one- (I) and two-step (II) mechanisms (see text).

		SIA	di-SIA
E_f	$\langle 110 \rangle$	3.64	6.56 (1nn), 7.11 (2nn), 6.91 (3nn)
	$\langle 111 \rangle$	4.34	7.31 (1nn)
	$\langle 100 \rangle$	4.64	7.65 (1nn), 8.48 (2nn)
E_m	Calc.	0.34	0.42 (I), 0.43 (II)
	Exp.	0.30 (0.32[a])	0.42

[a]Deduced from rotation energy.

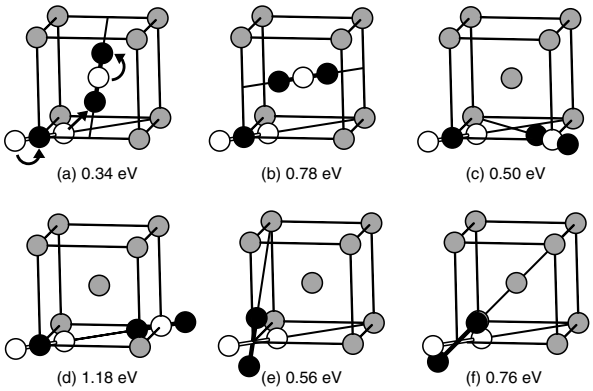

FIG. 2. Schematic representation of the translation and/or rotation jumps of SIAs studied here with their respective activation energies: (a) translation rotation to first neighbor; (b) translation to first neighbor; (c) jump to second neighbor; (d) jump to third neighbor; (e) 60° on-site rotation; (f) [110]-to-[111] on-site rotation. White and black spheres indicate initial and final positions of SIAs, their jumps are indicated by arrows in (a).

migration energy, E_m, of 0.34 eV in excellent agreement with the experimental value of 0.30 ± 0.03 eV [4]. This mechanism, proposed by Johnson [25], implies three-dimensional migration of SIAs in agreement with experimental evidence. Pure translation jumps to nearest neighbor and to third neighbor [26] [Figs. 2(b) and 2(d)] have also been proposed for bcc metals [3]. They appear to be much less favorable with $E_m = 0.78$ and 1.18 eV respectively. On the other hand, the second nearest-neighbor jump [Fig. 2(c)], with a saddle point near the tetrahedral configuration, is rather favorable with $E_m = 0.50$ eV. This mechanism will be activated at temperatures comparable to that for vacancy migration.

Concerning on-site rotations, the easiest path is found for the 60° rotation from [110] to [101] [Fig. 2(e)] with a barrier of 0.56 eV, i.e., larger than the translation-rotation migration energy, $E_m = 0.34$ eV. Very accurate values of rotation activation energies have been determined experimentally by magnetic aftereffect or internal friction measurements [4], which yield $E_{\text{rot}} = 0.32 \pm 0.01$ eV. The present calculations allow one to alleviate the uncertainty on the rotations responsible for E_{rot}: they clearly correspond to translation rotations rather than to on-site rotations. The measurement of E_{rot} therefore also provides a determination of the migration energy.

The rotation path between ⟨110⟩ and ⟨111⟩ dumbbells [Fig. 2(f)] shows that the ⟨111⟩ dumbbell is nearly unstable with a barrier towards ⟨110⟩ configuration of less than 0.05 eV. This near-instability implies that, assuming that ⟨111⟩ dumbbells are formed, they will rapidly fall into the ⟨110⟩ configuration rather than diffuse over appreciable distances in the ⟨111⟩ direction.

In order to investigate whether magnetism may explain why the behavior of SIAs in Fe is so different from that in other bcc transition metals (V, Nb, Ta, Cr, Mo, W), we have calculated the local magnetic moments on various

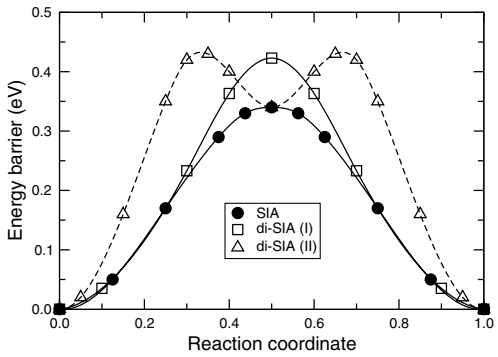

FIG. 3. Energetic barrier along the migration pathways for SIAs (nearest-neighbor translation-rotation mechanism) and di-SIAs (one- and two-step mechanisms).

stable and saddle-point SIA configurations by Mulliken population analysis. Local antiferromagnetism with respect to surrounding atoms is found in some low-energy SIA configurations such as ⟨110⟩ dumbbell in agreement with Ref. [8] ($-0.4\mu_B$ on each dumbbell atom) and tetrahedral SIA ($-1.0\mu_B$), as well as for the saddle-point configurations of the two most favorable migration pathways and of the 60° on-site rotation ($-0.9\mu_B$, $-1.0\mu_B$, and $-0.6\mu_B$, respectively). In other configurations only well known reductions of local magnetism are observed due to the smaller interatomic distances. This analysis suggests that local antiferromagnetism may indeed contribute to energetic stability.

Concerning di-SIAs we have investigated a series of possible configurations of parallel dumbbells—⟨110⟩ and ⟨100⟩ dumbbells at first and second nearest neighbor and ⟨111⟩ dumbbells at nearest neighbor—as well as a few nonparallel ones such as the [110] and [101] third-nearest neighbor dumbbells (see intermediate configuration in Fig. 4). The ⟨110⟩ configurations are found to be significantly more stable, with a minimum for nearest-neighbor dumbbells (see Table II). This result being again at variance with empirical potential predictions of the ⟨111⟩ configuration [6,7,14], the question of the orientation of tri-SIAs or larger SIA clusters is open, with a possibility for them to adopt also the ⟨110⟩ orientation for kinetic or

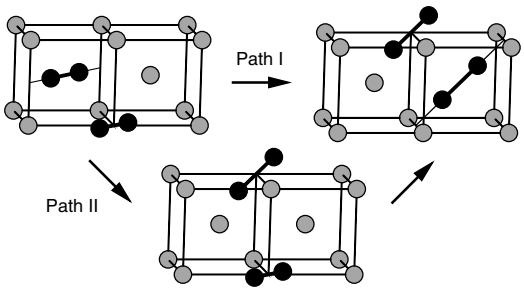

FIG. 4. Schematic representation of the initial, (intermediate), and final configurations for the migration of di-SIAs by simultaneous (I) or successive (II) SIA jumps investigated here.

energetic reasons. Their growth and/or reactions will directly impact the orientation of small SIA loops [13].

For the migration between two equivalent stable di-SIA configurations, we considered two mechanisms involving for each SIA the mechanism identified above for isolated SIAs: the two SIAs can jump either successively, as proposed in Ref. [25], or simultaneously (see Fig. 4). Note that for di-SIAs four distinct final configurations are possible instead of eight for isolated SIAs. The migration energy is found to be almost the same for the two mechanisms (0.42 and 0.43 eV). The midway configuration of the two-step mechanism is metastable, 0.35 eV above the stable configuration (see Fig. 3). Since the migration energy is smaller than the binding energy between SIAs (0.72 eV), it is obviously smaller than the dissociation energy, and therefore di-SIAs can migrate without total dissociation [10]. Moreover, the present results confirm that the abrupt resistivity change at 150–200 K (stage II) in resistivity recovery experiments, attributed to the migration of small SIA clusters with an activation energy of 0.42 eV [10], is indeed due—at least partly—to di-SIA migration. The perfect agreement between calculated and experimental activation energies indeed strongly supports this interpretation.

In summary, the present *ab initio* calculations are in agreement with experiments for the SIA configuration, namely, the $\langle 110 \rangle$ dumbbell and the SIA migration energy, and they allow one to make the following conclusions: (i) the $\langle 111 \rangle$ dumbbell is nearly unstable and it is therefore not expected to play any appreciable role; (ii) the di-SIA stable structure is made of parallel nearest-neighbor $\langle 110 \rangle$ dumbbells; (iii) the dominant migration mechanisms for SIAs and di-SIAs have been identified to be made of nearest-neighbor translation-rotation jumps showing that their diffusion is three dimensional; (iv) the second nearest-neighbor jump is proposed as a complementary mechanism for SIA migration with $E_m^{2nn} = 0.5$ eV; (v) the experimental SIA rotation energy corresponds to the translation-rotation mechanism involved in SIA migration; and (vi) di-SIAs are evidenced to contribute to recovery stage II, with migration energy of 0.42 eV in perfect agreement with the value deduced from experiments. In view of this new energetic landscape, the accepted pictures of the stability, mobility, and reactions of small SIA clusters and of SIA-loop nucleation should clearly be revisited.

We acknowledge A. Barbu, J. L. Bocquet, J. Dalla Torre, B. Legrand, V. Oison, and M. Weissmann for helpful discussions and G. Jomard for providing the STAMP code with an implementation of the Fe MEAM potential. This work was supported by the PERFECT European Integrated Project under Contract No. FI60-CT-2003-508840 and by Spain's MCyT under Grant No. BFM2003-03372-C03-01.

[1] R. S. Averbach and T. Diaz de la Rubia, Solid State Phys. **51**, 281 (1998); T. Diaz de la Rubia, H. M. Zbib, T. A. Khraishi, B. D. Wirth, M. Victoria, and M. J. Caturla, Nature (London) **406**, 871 (2000).
[2] P. Ehrhart, K. H. Robrock, and H. R. Schober, in *Physics of Radiation Effects in Crystals*, edited by R. A. Johnson and A. N. Orlov (Elsevier, Amsterdam, 1986), p. 63.
[3] W. Schilling, J. Nucl. Mater. **69–70**, 465 (1978).
[4] H. Schultz, in *Atomic Defects in Metals*, Landolt-Börnstein New Series, Group III, Vol. 25 (Springer-Verlag, Berlin, 1991), p. 115.
[5] J. Marian, B. D. Wirth, A. Caro, B. Sadigh, G. R. Odette, J. M. Perlado, and T. Diaz de la Rubia, Phys. Rev. B **65**, 144102 (2002).
[6] N. Soneda and T. Diaz de la Rubia, Philos. Mag. A **81**, 331 (2001).
[7] B. D. Wirth, G. R. Odette, D. Maroudas, and G. E. Lucas, J. Nucl. Mater. **244**, 185 (1997).
[8] C. Domain and C. S. Becquart, Phys. Rev. B **65**, 024103 (2002).
[9] EAM potentials for Fe fitted to *ab initio* SIA formation energies have been newly proposed: M. I. Mendelev, S. Han, D. J. Srolovitz, G. J. Ackland, D. Y. Sun, and M. Asta, Philos. Mag. **83**, 3977 (2003). SIA migration and SIA-cluster properties remain to be tested.
[10] S. Takaki, J. Fuss, H. Kugler, U. Dedek, and H. Schultz, Radiat. Eff. **79**, 87 (1983).
[11] T. M. Robinson, Phys. Status Solidi (a) **75**, 243 (1983).
[12] J. Marian, B. D. Wirth, and J. M. Perlado, Phys. Rev. Lett. **88**, 255507 (2002).
[13] B. L. Eyre and R. Bullough, Philos. Mag. **12**, 31 (1965).
[14] Yu. N. Osetsky, D. J. Bacon, A. Serra, B. N. Singh, and S. I. Golubov, J. Nucl. Mater. **276**, 65 (2000).
[15] J. M. Soler, E. Artacho, J. D. Gale, A. Garcia, J. Junquera, P. Ordejon, and D. Sanchez-Portal, J. Phys. Condens. Matter **14**, 2745 (2002).
[16] P. Ordejón, Phys. Status Solidi (b) **217**, 335 (2000).
[17] J. Izquierdo, A. Vega, L. C. Balbas, D. Sanchez-Portal, J. Junguera, E. Artacho, J. M. Soler, and P. Ordejon, Phys. Rev. B **61**, 13 639 (2000).
[18] S. Han, L. A. Zepeda-Ruiz, G. J. Ackland, R. Car, and D. J. Srolovitz, Phys. Rev. B **66**, 220101(R) (2002).
[19] The volume of the cell is fixed to $N + 1$ (or $N + 2$ for di-SIAs) times the bulk equilibrium volume ($N = 54$ or 128), as explained in F. Willaime, J. Nucl. Mater. **323**, 205 (2003).
[20] V. Oison and F. Willaime (to be published).
[21] G. J. Ackland, D. J. Bacon, A. F. Calder, and T. Harry, Philos. Mag. A **75**, 713 (1997).
[22] B. J. Lee, M. I. Baskes, H. Kim, and Y. K. Cho, Phys. Rev. B **64**, 184102 (2001).
[23] H. J. Wollenberger, in *Physical Metallurgy*, edited by R.W. Cahn and P. Haasen (Elsevier, Amsterdam, 1996), 4th ed., p. 1621.
[24] T. R. Mattsson and A. E. Mattsson, Phys. Rev. B **66**, 214110 (2002).
[25] R. A. Johnson, Phys. Rev. **134**, A1329 (1964).
[26] The saddle point is close to octahedral configuration.